

DLRMamba: Distilling Low-Rank Mamba for Edge Multispectral Fusion Object Detection

Qianqian Zhang, Leon Tabaro, Ahmed M. Abdelmoniem, and Junshe An

Abstract—Multispectral fusion object detection is a critical task for edge-based maritime surveillance and remote sensing, demanding both high inference efficiency and robust feature representation for high-resolution inputs. However, current State Space Models (SSMs) like Mamba suffer from significant parameter redundancy in their standard 2D Selective Scan (SS2D) blocks, which hinders deployment on resource-constrained hardware and leads to the loss of fine-grained structural information during conventional compression. To address these challenges, we propose the Low-Rank Two-Dimensional Selective Structured State Space Model (Low-Rank SS2D), which reformulates state transitions via matrix factorization to exploit intrinsic feature sparsity. Furthermore, we introduce a Structure-Aware Distillation strategy that aligns the internal latent state dynamics of the student with a full-rank teacher model to compensate for potential representation degradation. This approach substantially reduces computational complexity and memory footprint while preserving the high-fidelity spatial modeling required for object recognition. Extensive experiments on five benchmark datasets and real-world edge platforms, such as Raspberry Pi 5, demonstrate that our method achieves a superior efficiency-accuracy trade-off, significantly outperforming existing lightweight architectures in practical deployment scenarios.

Index Terms—Distillation, Mamba, Multispectral fusion, Object detection.

I. INTRODUCTION

OBJECT detection plays an important role in various fields, including maritime surveillance [1], remote sensing [2], and urban security tasks [3]. In these scenarios, objects are highly susceptible to environmental noise and variations in illumination conditions. While traditional single-spectral detection methods have established a solid foundation, they frequently suffer performance degradation in complex

environments [4]. To address this, fusing multi-spectral information has emerged as a robust alternative, as it effectively complements object features by integrating diverse physical properties, such as thermal signatures and textural details [5], [6], [7].

The practical deployment of such tasks typically requires execution on resource-constrained edge devices. Moreover, with the rapid advancement of imaging sensors, the resolution of input images has increased significantly, demanding higher inference efficiency [4], [8]. Compared to Convolutional Neural Networks (CNNs) and Vision Transformers (ViTs), the recently proposed State Space Model (Mamba) architecture [9], [10], has demonstrated a superior ability to maintain long-range spatial modeling while achieving linear computational complexity. This characteristic makes Mamba an ideal backbone for processing high-resolution images on efficiency-sensitive platforms.

However, we observe that standard 2D Selective Scan (SS2D) blocks exhibit significant technical limitations when handling dense spatial dependencies. Specifically, the standard SS2D layers often exhibit substantial parameter redundancy, which severely limits their deployment on resource-constrained edge hardware. A well-established solution to this redundancy is currently missing because existing compression techniques often fail to preserve the fine-grained structural information essential for object detection. The technical reason lies in the misalignment between parameter reduction and the need for high-fidelity spatial representation in SSMs.

In this paper, we are motivated to develop a more efficient recognition framework that compresses structural information without sacrificing discriminative power.

Low Rank Two Dimensional Selective Structured State Space Model for Efficient Recognition. Traditional state space models such as Mamba encounter significant technical hurdles in visual tasks, specifically excessive computational redundancy and overparameterized structures that impede deployment on resource-constrained edge devices. To address these limitations, we propose a Low-Rank two dimensional state space (SS2D) modeling approach, termed Low Rank SS2D, specifically tailored for visual recognition. Instead of constructing state transitions using full rank matrices, the core transition component is reformulated via matrix factorization. As shown in Fig. 1. The primary technical advantage of this method lies in its ability to exploit the intrinsic sparsity and low-rank characteristics of visual features. Consequently, the proposed architecture substantially reduces model parameters and computational complexity while preserving the capacity to model long-range spatial dependencies.

This work was supported in part by the China Scholarship Council (CSC) program (Project ID: 202504910309) and Research on the Working Principle and Application of Intelligent Satellite Brain under the National Key Research and Development Program of China (Project ID: 2022YFF0503900) and UKRI EPSRC Grant Reference EP/X035085/1. This work was completed entirely while Qianqian Zhang was a visiting researcher at Queen Mary University of London, UK. (Corresponding authors: Qianqian Zhang)

Qianqian Zhang is with the National Space Science Center, Chinese Academy of Sciences, Beijing, 101499, China, the School of Computer Science and Technology, University of Chinese Academy of Sciences, Beijing, 100049, China, and the School of Electronic Engineering and Computer Science, Queen Mary University of London, London, E1 4NS, UK (e-mail: zhangqianqian21@mails.ucl.ac.uk).

Leon Tabaro and Ahmed M. Abdelmoniem are with the School of Electronic Engineering and Computer Science, Queen Mary University of London, London, E1 4NS, UK (e-mails: l.tabaro@qmul.ac.uk, ahmed.sayed@qmul.ac.uk).

Junshe An is with the National Space Science Center, Chinese Academy of Sciences, Beijing, 101499, China, and the School of Astronomy and Space Science, University of Chinese Academy of Sciences, Beijing, 100049, China (e-mail: anjunshe@nssc.ac.cn).

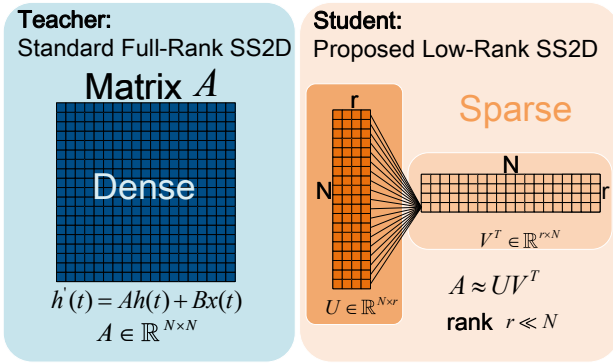


Fig. 1. Structural comparison of full-rank vs. low-rank SS2D. By significantly reducing computational overhead while maintaining representative power, the low-rank design opens up new avenues for efficient vision computing on resource-constrained edge devices.

Structure Aware Distillation Tailored for Low Rank SS2D.

To mitigate the potential degradation in representational capacity induced by low-rank compression, we introduce a structure-aware distillation strategy for the Low Rank SS2D framework. Unlike conventional distillation methods, our approach leverages a full-rank teacher model to guide the low-rank student model via a multidimensional loss function. This objective comprises singular value decomposition (SVD)-aligned distillation, hidden-state sequence distillation, and feature-reconstruction distillation. The technical advantage of this method is its ability to precisely compensate for information loss caused by low-rank modeling. By compelling the student model to emulate the teacher's internal state-transition dynamics rather than merely matching final outputs, this paradigm extends beyond simple knowledge compression. Aligning the internal latent state spaces enables lightweight models to reproduce the complex spatiotemporal reasoning capabilities of large-scale models.

Comprehensive Cross Platform Validation with Real World Edge Deployment. Existing lightweight visual models often emphasize theoretical reductions in computational complexity but lack empirical validation of real-world inference latency across heterogeneous platforms. We conduct extensive experiments on five benchmark datasets to validate the effectiveness of the proposed approach. In addition to measuring real-time inference performance on high-end GPUs, including the NVIDIA A100 and NVIDIA GeForce RTX 4090, we implement and benchmark deployment on edge platforms such as the Raspberry Pi 5. Experimental results demonstrate that our method maintains high recognition accuracy while achieving efficient inference on computationally constrained edge devices. These findings validate the practical applicability of the proposed framework in real-world scenarios.

In summary, this article makes the following contributions.

- We propose a novel Low Rank SS2D architecture that significantly reduces computational redundancy while preserving the ability to model long-range spatial dependencies, enabling efficient visual recognition on edge devices.
- We introduce a structure aware distillation strategy tailored for low rank models, which effectively compensates

for information loss and allows lightweight models to replicate the complex reasoning capabilities of larger models.

- We conduct comprehensive experiments across multiple benchmark datasets and real world edge platforms, demonstrating that our method achieves high accuracy while maintaining efficient inference, validating its practical applicability in real world scenarios.
- To the best of our knowledge, this is among the few works to systematically address the challenges of deploying state space models for visual recognition on resource-constrained edge devices, providing a new paradigm for efficient model design and deployment in this domain.

II. RELATED WORK

A. Multispectral Fusion for Object Detection

Recently, in the field of remote sensing imaging (RSI), multispectral fusion has attracted increasing attention for improving object detection performance under complex environmental conditions. Unlike natural scene images, remote sensing data often exhibit large-scale variations, occlusion, and severe background interference [11]. While recent single-modal RGB detectors have advanced through multiscale feature reconstruction and dynamic receptive field modeling [12], [13], [14] their performance remains inherently fragile and suffers from significant degradation under variations in illumination, nighttime, or adverse weather conditions. In contrast, infrared (IR) images captures thermal radiation patterns that are largely invariant to lighting conditions and can highlight object contours even in challenging environments, yet generally exhibits lower spatial resolution, reduced texture detail, and limited semantic richness compared to RGB images [15]. These complementary characteristics naturally motivate the integration of visible and infrared modalities for more reliable object detection in RSI technologies [16], [17], [18], [19]. To realize effective fusion, early deep learning-based approaches predominantly employ convolutional neural networks (CNNs) to extract hierarchical spatial features and fine-grained local patterns. SuperYOLO [4] introduces a pixel-level symmetric multimodal fusion module to efficiently combine RGB and IR inputs. However, the locality bias induced by the fixed receptive field size in CNN-based methods limits their ability to learn global contextual information. And so to overcome these limitations, several hybrid architectures combining convolutional backbones with attention-based interaction modules have been proposed to explicitly capture long-range dependencies and address the challenges of intermodal discrepancies and intramodal variability in RGB-IR fusion [20], [21], [22], [23], [24].

Unfortunately, in spite of the ubiquity and strong performance of Transformer architectures in modelling long-range dependencies, the $\mathcal{O}(N^2)$ complexity of the attention mechanism is extremely wasteful, and becomes a significant bottleneck for many applications involving long sequences such as high-resolution sensing images [9]. This redundancy results in both high memory consumption and high inference latency, whereas systems for such real-world applications often demand real-time responses with low latency and inference cost.

B. Vision Mamba for Efficient Visual Representation

Recently, Mamba [9], built on Structured State-Space Sequence Models (S4) [25], has emerged as a promising class of architectures for sequence modelling that addresses the inefficiency of CNNs and Transformers. By maintaining a fixed-size hidden-state representation, the Mamba model scales linearly with the input sequence length while preserving comparable expressive capacity through an adaptive selective-scan mechanism. VMamba [10] extends this framework to visual tasks through the 2D Selective Scan (SS2D) mechanism, effectively capturing long-range spatial dependencies. Recently, Vision Mamba [26], and SS2D-based architectures have been progressively introduced into multispectral remote sensing tasks [27], [28], [29]. DMM [28] introduces a disparity-guided selective scanning to mitigate intermodal discrepancies in oriented remote sensing detection. More recently, MVMamba [29] integrates state-space duality (SSD) mechanisms with multiscale fusion to enhance small-object detection performance in high-resolution remote sensing imagery.

Despite these advances, existing Mamba-based detection frameworks primarily focus on improving representation capability and cross-modal fusion performance, whereas comparatively less attention has been paid to the structural efficiency of the Mamba operator when deployed on resource-constrained edge devices such as smart satellites and drones, which often have limited memory and processing power. This work departs from prior efforts by shifting the focus to developing a compact yet expressive state-space modeling framework tailored for efficient multispectral object detection under edge-deployment conditions.

C. Model Compression and Knowledge Distillation for Edge Deployment

While modern deep neural networks (DNNs) have significantly advanced aerial image analysis, their high computational demands can make them prohibitive for deployment on resource-limited devices such as mobile phones and embedded systems. To mitigate this challenge, a long-standing strategy has been to exploit the redundancy of overparameterized networks by replacing dense linear transformations with low-rank factorizations [30], [31].

1) *Low Rank Decomposition*: Formally, low-rank decomposition factorizes a large matrix $W \in \mathbb{R}^{m \times n}$ into two smaller matrices $U \in \mathbb{R}^{m \times k}$ and $V \in \mathbb{R}^{k \times n}$, such that $W = UV$, where $k \ll m$ and $k \ll n$. This reduces the parameter complexity from mn to $k(m+n)$. Such techniques have been extensively studied for compressing various components of neural architectures and, in recent years, have been widely adopted for compressing large pretrained models [32], [33], thereby demonstrating significant reductions in computational and memory footprints.

Moreover, recent theoretical and empirical studies have revealed that deep networks exhibit intrinsic spectral concentration and rank diminishing behavior across layers, leading to low-dimensional feature representations [30], [34]. This suggests that much of the expressive capacity of overparameterized models is concentrated in a small set of dominant singular directions.

2) *Knowledge Distillation*: Knowledge Distillation (KD) has emerged as a pivotal technique for deploying large-scale models onto edge devices without substantial performance degradation [35]. Established KD methodologies are generally categorized into response-based, feature-based, and relation-based distillation [36]. Notably, knowledge distillation has been widely applied in remote sensing tasks to improve the performance of lightweight detection models [24], [37], [38], [39], [40]. IRKD [38] proposes a feature-based distillation framework tailored for infrared small-target detection, in which channel-spatial attention masks selectively transfer informative features from the teacher to the student network. Closely related to this work, TDKD-Net [37] introduces a tensor decomposition-based compression strategy for UAV object detection and employs response-based distillation to compensate for accuracy degradation caused by low-rank convolutional approximation.

III. BASELINE ARCHITECTURE

The baseline framework mainly consists of three functional components: the Pixel-level Multi-modal Fusion Module, the State Space 2D Backbone, and the Detection Network with a YOLOv8n[41] Head. In the subsequent subsections, we first give a brief introduction to the SS2D mechanism, then elaborate on each component of the baseline in detail.

A. Preliminaries: SS2D Mechanism

As outlined in the baseline framework, the State Space 2D (SS2D) backbone serves as the core for feature extraction. This subsection first reviews the foundational State Space Models (SSM), specifically Mamba [9], and then elaborates on how VMamba [10] extends this mechanism to 2D visual data through the SS2D module.

1) *Mamba: Selective State Space Modeling*: SSMs map an input sequence $x(t) \in \mathbb{R}$ to an output $y(t) \in \mathbb{R}$ via a hidden state $h(t) \in \mathbb{R}^N$. In a continuous-time 1-D context, the system is defined by linear ordinary differential equations (ODEs):

$$\begin{aligned} h'(t) &= \mathbf{A}h(t) + \mathbf{B}x(t), \\ y(t) &= \mathbf{C}h(t), \end{aligned} \quad (1)$$

where $\mathbf{A} \in \mathbb{R}^{N \times N}$ is the state transition matrix, $\mathbf{B} \in \mathbb{R}^{N \times 1}$ is the input coefficient vector, and $\mathbf{C} \in \mathbb{R}^{1 \times N}$ serves as the output coefficient vector.

To handle discrete sequences, Mamba [9] introduces a selective mechanism by making these matrices dynamically dependent on the input. It discretizes the system using a time step parameter Δ via the zero-order hold (ZOH) method:

$$\begin{aligned} \bar{\mathbf{A}} &= \exp(\Delta \mathbf{A}), \\ \bar{\mathbf{B}} &= (\Delta \mathbf{A})^{-1}(\exp(\Delta \mathbf{A}) - \mathbf{I}) \cdot \Delta \mathbf{B}. \end{aligned} \quad (2)$$

After discretization, the recurrence is formulated as:

$$\begin{aligned} h_k &= \bar{\mathbf{A}}h_{k-1} + \bar{\mathbf{B}}x_k, \\ y_k &= \mathbf{C}h_k. \end{aligned} \quad (3)$$

This design ensures linear complexity and efficient training; however, its sequential scanning is inherently 1-D, making it suboptimal for 2-D spatial data like images, which lack a predefined scan order.

2) *VMamba and SS2D Module*: To bridge the gap between 1-D scanning and 2-D spatial information, VMamba [10] introduces the Visual State Space (VSS) block. Its core component, the SS2D module, addresses the sequential scanning problem by traversing images across four different scan paths as shown in Fig. 2 (b). This ensures that each pixel captures dependencies from multiple directions, effectively modeling local textures and global structures.

Furthermore, the VSS block enhances computational efficiency by utilizing a structure of network branches and twin residual modules instead of traditional multiplicative branches, Fig. 2 (a).

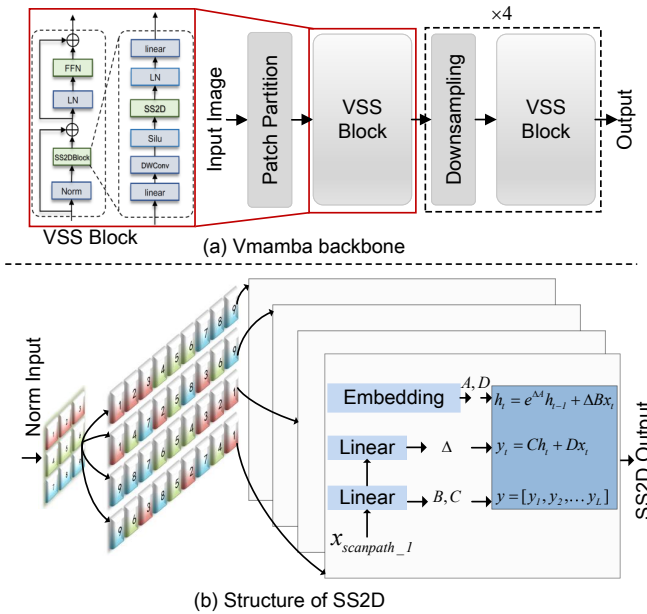


Fig. 2. Overview of the VMamba backbone and SS2D module.

B. Pixel-level Multi-modal Fusion

A primary challenge in multi-modal object detection is the environmental sensitivity of individual sensors: RGB images exhibit degraded performance in low-light conditions, whereas infrared (IR) images lack rich texture information. Existing methods typically perform fusion at the deep feature level, which may lead to the loss of fine-grained spatial information. To address this issue, we draw on the pixel-level fusion module proposed in [42] to construct a unified and robust input representation at the earliest stage of the network (As shown in Fig. 3). The Pixel-level Multi-modal Fusion module integrates complementary information from different sensors to generate a unified representation I^f . The detailed workflow is summarized as follows:

Given a pair of visible–infrared images, we denote the visible image as $I^v \in \mathbb{R}^{H \times W \times C}$ and the infrared image as $I^i \in \mathbb{R}^{H \times W \times C}$, where H , W , and C represent the height, width, and number of channels of the input images, respectively.

The two modalities are fused at the pixel level through the operator $\mathcal{F}_{\text{fusion}}$.

The fused multi-modal representation $I^f \in \mathbb{R}^{H \times W \times C_{\text{in}}}$ is produced, where C_{in} denotes the channel depth of the fused feature map.

Mathematically, the fusion operation is formulated as:

$$I^f = \mathcal{F}_{\text{fusion}}(I^v, I^i) \quad (4)$$

By performing pixel-level fusion, fine-grained details critical for object detection can be preserved, thereby significantly enhancing the model’s robustness under extreme illumination variations and sensor noise.

IV. THE PROPOSED FRAMEWORK

The proposed framework aims to achieve efficient multi-modal object detection by compressing the two-dimensional state space model (SS2D) while maintaining high-fidelity feature representation. While leveraging the baseline’s pixel-level multi-modal fusion and task-specific Detection Head, the framework introduces two pivotal enhancements: Low-Rank SS2D Representation and Structure-Aware Distillation, ensuring high-fidelity feature extraction despite the reduced model footprint. As shown in Fig. 3.

A. Low-Rank 2D Selective Structured State Space Model

A remaining bottleneck in deploying SS2D on edge devices is the high computational complexity of the full-rank system matrix A . In standard SS2D, the hidden state transition entails dense matrix operations that pose significant challenges for real-time inference. To mitigate this, we introduce the Low-Rank SS2D module, which leverages low-rank factorization to reduce the parameter count while preserving a large global receptive field.

The Low-Rank SS2D module replaces the standard full-rank state transition with a factorized alternative. The detailed design is as follows:

Based on the Singular Value Decomposition (SVD) property, the full-rank system matrix $A \in \mathbb{R}^{N \times N}$ is decomposed into two low-rank matrices $U \in \mathbb{R}^{N \times r}$ and $V \in \mathbb{R}^{N \times r}$, where $r \ll N$.

Instead of computing Ah_{t-1} , the student model computes the transition in two smaller steps: first projecting the previous state h_{t-1} into a low-dimensional subspace via V^T , and then projecting it back via U .

The discretized state-space equation for the student model is updated as:

$$h_t^s = (UV^T)h_{t-1}^s + Bx_t \quad (5)$$

This low-rank structure significantly accelerates inference speed on resource-constrained hardware while maintaining the capability to model long-range dependencies inherent in the SS2D architecture.

B. Structure-Aware Distillation Tailored for Low-Rank SS2D

Simply reducing the rank of the SS2D module results in a performance gap relative to the full-rank teacher model. The

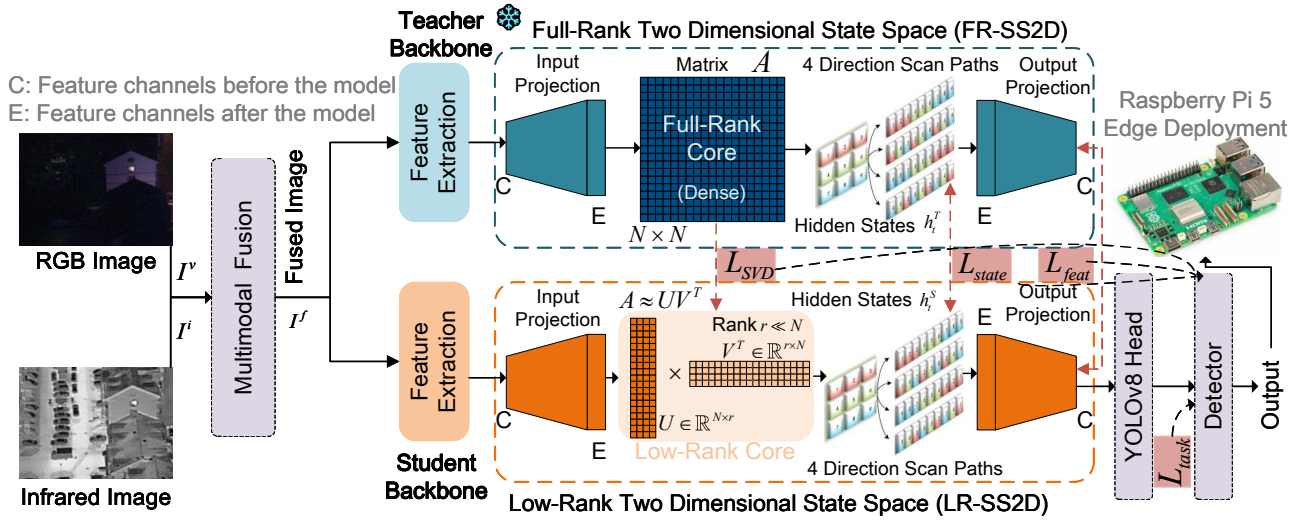


Fig. 3. Overview of the proposed DLRMamba framework. The proposed framework consists of four core components: (1) A pixel-level multispectral modality fusion module, which is designed to effectively fuse and process visible and infrared spectral information; (2) Low-Rank Structured State Space Modeling (Low-Rank SS2D), which is integrated to realize model lightweighting; (3) A structure-aware distillation (SAD) mechanism, including Singular Value Decomposition (SVD) Alignment (Matrix-level Distillation), Hidden State Sequence Alignment (Dynamic Distillation), and Feature Reconstruction (Output-level Distillation), which is proposed to compensate for performance degradation induced by model compression; (4) A detection head, which is used to output the final detection results.

key challenge lies in compensating for information loss during compression. We propose a Structure-Aware Distillation module to guide the student model in inheriting the teacher's internal spatio-temporal dynamics and weight structures.

The Structure-Aware Distillation module utilizes a triple-alignment strategy to supervise the student model. The detailed implementation steps are as follows:

1) *SVD Alignment (Matrix-level Distillation)*: We align the student's low-rank matrices U_s, V_s with the principal singular components of the teacher's matrix A_t . Specifically, we denote the aligned principal singular components of the teacher as U_t and V_t . The corresponding loss is then defined as:

$$\mathcal{L}_{SVD} = \|U_s - U_t\|_F^2 + \|V_s - V_t\|_F^2 \quad (6)$$

where $U_t = (U_t \sqrt{\Sigma_t})_{1:r}$ and $V_t = (V_t \sqrt{\Sigma_t})_{1:r}$.

2) *Hidden state sequence Alignment (Dynamic Distillation)*: This is the key to capturing long-range dependencies. SS2D generates a series of hidden states $H = \{h_1, h_2, \dots, h_L\}$ when scanning an image. We require the state trajectory H_{stud} of the Student to mimic the state trajectory H_{teach} of the Teacher, ensuring that both respond consistently to dynamic features:

$$\mathcal{L}_{\text{state}} = \frac{1}{L} \sum_{t=1}^L \text{MSE}(h_t^s, P(h_t^t)) \quad (7)$$

where P is a dimension-adaptive projection layer used to align the potentially different state dimensions of the Teacher and the Student. MSE is the Mean Squared Error, which measures the average squared difference between the student and teacher hidden states across all time steps. By minimizing this loss, we encourage the student model to closely follow the temporal dynamics of the teacher model, thus preserving the long-range dependencies that are crucial for accurate feature representation in SS2D.

3) *Feature reconstruction (Output-level Distillation)*: To ensure the semantic consistency of the final feature map, we perform reconstruction distillation on the output Y of the SS2D module. We minimize the distance between the output feature maps Y_t and Y_s to guarantee semantic consistency, with the loss defined as:

$$\mathcal{L}_{\text{feat}} = \|Y_t - Y_s\|_2^2 \quad (8)$$

Structure-Aware Distillation, specifically tailored to the Low-Rank SS2D module, ensures structural fidelity during compression. By aligning hidden-state trajectories and weight-decomposition manifolds, the student model effectively captures the teacher's fine-grained reasoning logic. This multi-dimensional supervision mechanism bridges the performance gap typically introduced by low-rank approximations.

C. Task Specific Detector

After extracting efficient multi-modal features, the final challenge lies in translating these representations into accurate object localizations and classifications. To address this, we employ a Decoupled Detection Head to process the task.

The Detection Head processes the multi-scale feature pyramid generated by the Low-Rank SS2D backbone. The workflow is as follows:

First, the module takes as input multi-scale features denoted as $P = \{P_3, P_4, P_5\}$, where each element corresponds to a feature map at a different spatial scale; second, each feature map is fed into two parallel branches, with one branch dedicated to Bounding Box Regression and the other to Class Probability prediction; finally, the head outputs the final detection results $\hat{Y}_{\text{det}} = \{\hat{B}_{\text{box}}, \hat{C}_{\text{cls}}\}$, encompassing both bounding box coordinates and class probabilities.

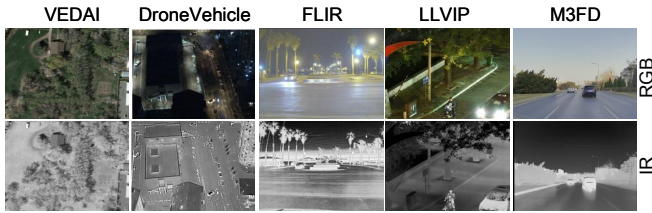


Fig. 4. Sample RGB-IR pairs from five datasets (top: RGB; bottom: IR).

The total training objective is formulated as the combination of the primary detection task loss and auxiliary distillation losses:

$$\mathcal{L}_{Total} = \lambda_1 \mathcal{L}_{Task}(\hat{Y}_{det}, GT) + \lambda_2 \mathcal{L}_{SVD} + \lambda_3 \mathcal{L}_{state} + \lambda_4 \mathcal{L}_{feat} \quad (9)$$

where $\lambda_1 = 1.0$, $\lambda_2 = 0.5$, $\lambda_3 = 0.1$, and $\lambda_4 = 1.5$ denote the weighting coefficients for the corresponding losses, respectively.

The decoupled detection design facilitates faster convergence and enhances both precision and recall. Furthermore, integrating distillation losses into the overall objective function enables the detection head to leverage highly distilled, efficient features, ultimately yielding superior performance on devices.

V. EXPERIMENTAL RESULTS

In this section, we introduce the five datasets used for evaluation, the implementation details, the accuracy metrics, as well as extensive comparison experiments and ablation studies to verify the effectiveness of the proposed method.

A. Dataset

We evaluate our method on five widely used RGB-IR object detection datasets: VEDAI [43], FLIR [44], LLVIP [45], M3FD [46], and DroneVehicle [47]. Sample RGB-IR pairs from these five datasets, as shown in Fig. 4. These datasets encompass a diverse range of scenarios, including urban traffic, pedestrian detection, and aerial surveillance, providing a comprehensive benchmark for assessing the performance of our approach.

B. Implementation Details

The model is trained on a single NVIDIA RTX A100 GPU with 80GB of memory. In addition, we conduct inference tests on the NVIDIA RTX 4090 GPU and the Raspberry Pi 5 and compare the frames-per-second (FPS) performance across these three devices. We implement our algorithm using PyTorch, and adopt the SGD optimizer [48] with a momentum of 0.937 and a weight decay of 0.0005. The learning rate is set to 0.01, the batch size is 8, and the model is trained for 300 epochs. Since richer, more comprehensive object annotations are available for the infrared modality, we use the ground truth of IR images as the training labels.

C. Accuracy Metrics

mAP_{50} is adopted as the accuracy metric to evaluate the performance of different methods. It is calculated based on precision (P) and recall (R), which are defined as:

$$P = \frac{TP}{TP + FP}, \quad R = \frac{TP}{TP + FN} \quad (10)$$

where TP , FP , and FN represent the number of true positives, false positives, and false negatives, respectively. A detection is considered a TP if its Intersection over Union (IoU) with the ground truth exceeds a threshold of 0.5.

The average precision (AP) for a single category is the area under the precision-recall curve:

$$AP_{50} = \int_0^1 P(R) dR \quad (11)$$

Finally, mAP_{50} is defined as the mean of AP values across all N categories:

$$mAP_{50} = \frac{1}{N} \sum_{i=1}^N AP_{50,i} \quad (12)$$

Additionally, FPS and the number of parameters are used to assess real-time performance and computational cost.

D. Results Comparisons

1) *Superiority in Accuracy-Efficiency Trade-off*: Tables I and II demonstrate that our method achieves a superior trade-off between detection accuracy and model compactness.

To further validate the superiority of our approach, we provide a visual comparison of detection results in Fig. 5. While existing mainstream methods frequently suffer from various detection inaccuracies in challenging scenarios, our approach effectively handles tree occlusions and extremely dense scenes, whereas competing models often miss objects or confuse background textures with objects. These qualitative observations are consistent with our quantitative findings, demonstrating that our method not only reduces the parameter count but also learns more robust, semantically consistent feature representations in complex remote sensing environments.

2) *Generalization Across Multiple Benchmarks*: To evaluate the robustness of our proposed method, we conduct extensive evaluations across 5 challenging benchmarks. As summarized in Table III and Fig. 6.

3) *Superiority over pruning compression techniques*: Table IV shows that our Low-Rank SS2D method achieves a better balance between accuracy and efficiency compared with existing pruning compression approaches.

TABLE IV
COMPARISON OF OUR LOWRANK-SS2D METHOD WITH MAINSTREAM EXISTING LIGHTWEIGHTING METHODS ON THE VEDAI DATASET. (I: SS2D BASELINE; II: SS2D + PRUNING; III: SS2D + OUR LOWRANK; FPS MEASURED ON RASPBERRY PI 5, FP32; BLUE PARENTHESES INDICATE PERCENTAGE CHANGE RELATIVE TO I).

No.	SS2D replaced	Params (MB)↓	$mAP_{50}(\%)$ ↑	FPS↑
I	0	17.1	81.5	0.4
II	0	9.0 (-47.4%)	70.2 (-13.9%)	1.0 (+150.0%)
III	6	8.5 (-50.3%)	75.5 (-7.4%)	1.2 (+200.0%)

TABLE I
COMPARISONS OF DIFFERENT METHODS ON THE VEDAI DATASET. THE BEST RESULT IS SHOWN IN **BOLD** AND THE SECOND BEST IS SHOWN WITH UNDERLINE.

Method (Journal, Year)	Car	Pickup	Camping Car	Truck	Other	Tractor	Boat	Van	mAP ₅₀ (%) [↑]
DMM (TGRS 2025)[28]	84.2	78.8	79.0	65.7	56.2	72.3	<u>72.3</u>	72.5	75.0
C2DFF-Net (TGRS 2025)[21]	<u>91.8</u>	<u>85.9</u>	87.2	74.4	58.7	78.6	62.2	91.3	79.8
MRN_lite (TGRS 2025)[12]	92.2	87.7	<u>83.9</u>	73.9	<u>68.1</u>	<u>80.4</u>	54.9	72.1	76.7
LGA-YOLO (JSTARS 2025)[13]	89.4	<u>85.9</u>	74.1	<u>83.4</u>	59.9	86.0	62.4	<u>83.2</u>	<u>80.3</u>
SuperYOLO (TGRS 2023)[4]	91.1	85.7	79.3	70.2	57.3	<u>80.4</u>	60.2	76.5	75.1
Ours	91.5	81.0	82.0	91.9	78.2	80.0	91.9	81.3	84.7

TABLE II
COMPARISON OF DETECTION ACCURACY AND MODEL SIZE ON THE VEDAI DATASET. THE BEST RESULT IS SHOWN IN **BOLD** AND THE SECOND BEST IS SHOWN WITH UNDERLINE.

Method	mAP ₅₀ (%) [↑]	Δ mAP ₅₀ (Method - Ours)(%)	Parameters (M) [↓]	Δ Param (Method - Ours)(%)
DMM (TGRS 2025)[28]	75.00	-9.70	87.97	+83.53
C2DFF-Net (TGRS 2025)[21]	79.80	-4.90	6.58	+2.14
PG-DRFNet (TCSVT 2025)[14]	<u>84.06</u>	-0.64	26.60	+22.16
MRN_lite (TGRS 2025)[12]	76.70	-8.00	6.87	+2.43
DETR (JSTARS 2024)[20]	77.30	-7.40	72.36	+67.92
LGA-YOLO (JSTARS 2025)[13]	80.30	-4.40	10.83	+6.39
DKDNet (TGRS 2025)[24]	77.90	-6.80	19.20	+14.76
CrossModalNet (ESA 2025)[22]	79.30	-5.40	92.80	+88.36
SuperYOLO (TGRS 2023)[4]	75.10	-9.60	<u>5.10</u>	+0.66
Ours	84.70	0.00	4.44	0.00

TABLE III
COMPARISONS OF DIFFERENT METHODS ON FOUR DATASETS. THE BEST RESULT FOR EACH DATASET IS SHOWN IN **BOLD**, AND THE SECOND-BEST RESULT IS SHOWN IN UNDERLINE. THE PERFORMANCE GAP BETWEEN OUR METHOD AND THE BEST RESULT IS SHOWN IN BLUE.

Dataset	Method (Journal, Year)	mAP ₅₀ (%) [↑]	Dataset	Method (Journal, Year)	mAP ₅₀ (%) [↑]
FLIR	EI2Det (TCSVT 2025)[19]	80.2	LLVIP	EI2Det (TCSVT 2025)[19]	98.0
	MMI-Det (TCSVT 2024)[7]	79.8		DHANet (TGRS 2025)[49]	<u>97.7</u>
	ICAFusion (PR 2024)[17]	77.5		PSFusion (IF 2023)[16]	96.6
	PSFusion (IF 2023)[16]	75.8		YOLO-Adaptor (TIV 2024)[50]	96.5
	CDDFuse (CVPR 2023)[51]	75.5		PIAFusion (IF 2022)[52]	96.1
	DATFuse (TCSVT 2023)[53]	75.4		CDDFuse (CVPR 2023)[51]	95.7
	PIAFusion (IF 2022)[52]	75.3		IFCNN (IF 2020)[54]	95.5
	IFCNN (IF 2020)[54]	74.9		YOLO Fusion (PR 2022)[55]	95.4
	DHANet (TGRS 2025)[49]	74.3		MoE-Fusion (ICCV 2023)[56]	91.0
	GAFF (WACV 2021)[6]	72.9		DIVFusion (IF 2023)[57]	89.8
	YOLO Fusion (PR 2022)[55]	71.7		DM-Fusion (TNNLS 2024)[58]	88.1
Ours	<u>80.0</u> (-0.2)	Ours	97.5 (-0.5)		
M3FD	MMI-Det (TCSVT 2024)[7]	76.6	Drone Vehicle	CIAN (IF 2019)[5]	70.8
	ICAFusion (PR 2024)[17]	<u>71.9</u>		AR-CNN (TNNLS 2021)[59]	71.6
	PIAFusion (IF 2022)[52]	69.9		TSFADet (ECCV 2022)[60]	73.1
	PSFusion (IF 2023)[16]	69.7		C^2 Former (TGRS 2024)[18]	<u>74.2</u>
	CDDFuse (CVPR 2023)[51]	69.5		S^2 ANET (TGRS 2021)[61]	71.5
	IFCNN (IF 2020)[54]	69.0		MBNet (ECCV 2020)[62]	71.9
	Ours	76.6		Ours	76.5 (+2.3)



Fig. 5. Visual comparison of detection results produced by our and competing approaches on the VEDAI dataset under various challenging scenarios. Subfigures (a) and (d) illustrate detection performance in the presence of tree occlusions. Subfigure (b) presents results in an extremely dense scene containing numerous objects of different scales and categories. Subfigures (c) and (e) demonstrate cases where background objects exhibit high visual similarity to the objects. Red circles denote misclassified objects (incorrect category prediction), blue circles indicate false positives (detections of non-existent objects), and yellow circles represent missed detections of ground-truth objects.

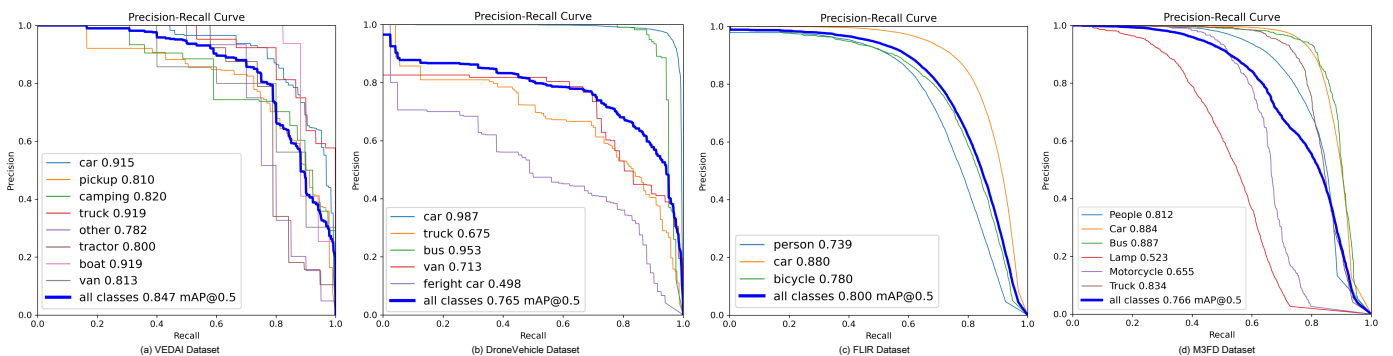


Fig. 6. Precision–Recall curves of our method on the VEDAI, FLIR, DroneVehicle, and M3FD datasets, showing the detection performance for each class. The LLVIP dataset contains only the person class, so its PR curve is not shown.

TABLE VI
EFFECT OF LOW-RANK DECOMPOSITION RANK RATIO ON DETECTION ACCURACY AND RASPBERRY PI 5 INFERENCE SPEED.

No.	Rank ratio	mAP ₅₀ (%) [↑]	FPS (Raspberry Pi 5) [↑]
I	0.65	80.20	0.64
II	0.60	79.60	0.98 (+53.1%)
III	0.55	76.71	1.13 (+76.6%)
IV	0.50	75.53	1.22 (+90.6%)

4) *Cross-Platform Efficiency Comparison*: Table V demonstrates the superior efficiency of our proposed method across diverse hardware architectures compared to the baseline. While our approach consistently outperforms the baseline on high-end GPUs, its most significant advantage is observed in resource-constrained environments. On the Raspberry Pi 5, our method achieves a 5.5 \times speedup in FPS.

TABLE V
INFERENCE SPEED ON DIFFERENT DEVICES.

No.	Method	Device	FPS [↑]	Inference time (ms) [↓]
I	Baseline	GPU A100	<u>41.88</u>	<u>23.88</u>
	Ours		43.59	22.94
II	Baseline	GPU 4090	<u>19.60</u>	<u>51.03</u>
	Ours		29.00	34.49
III	Baseline	Raspberry Pi 5	<u>0.42</u>	<u>2367.67</u>
	Ours		2.30	434.78

E. Ablation Study

1) *Relationship Between Low-Rank Decomposition Ratio and Inference Efficiency*: We analyze the sensitivity of our method to the low-rank decomposition ratio, a critical hyperparameter that balances detection accuracy and edge-device efficiency. As Table VI shows, performance varies predictably with the rank ratio. A high ratio (0.65, Row No. I) achieves the highest accuracy (80.20% mAP₅₀) but incurs a substantial computational cost on devices such as the Raspberry Pi 5 (0.64 FPS). Reducing the ratio markedly increases inference speed, with only minor degradation in accuracy. Under strict real-time constraints (Row No. IV), a ratio of 0.50 nearly doubles the FPS (+90.6%) while only reducing mAP₅₀ by 4.67%. These results demonstrate the method’s robustness to rank adjustments and its flexibility for tailoring performance to edge-resource limitations.

2) *Effectiveness of Structure-Aware Distillation for Low-Rank SS2D*: To meet the real-time requirement on resource-constrained devices, we deliberately adopt a more aggressive low-rank configuration. We rely on distillation and fine-tuning to restore performance.

Our ablation study, as shown in Table VII, underscores the critical role of the proposed structure-aware distillation in mitigating performance degradation and enhancing inference efficiency. Without the tailored distillation strategy (Row No. II), the initial low-rank decomposition of the SS2D layers reduces the parameter count from 17.1 MB to 8.5 MB.

TABLE VII
ABLATION STUDY OF MODEL COMPRESSION AND ACCELERATION ON VEDAI DATASET (FPS ON RASPBERRY PI 5, FP32). I: ORIGINAL SS2D (BASELINE); II: LOWRANK-SS2D WITHOUT DISTILLATION; III: LOWRANK-SS2D WITH DISTILLATION; IV: LOWRANK-SS2D WITH DISTILLATION AND FINE-TUNING. THE BEST RESULT IS SHOWN IN **BOLD** AND THE SECOND BEST IS SHOWN WITH UNDERLINE.

No.	SS2D replaced	Params (MB) [↓]	mAP ₅₀ (%) [↑]	FPS [↑]
I	0	17.1	<u>81.5</u>	0.4
II	6	<u>8.5</u>	75.5	<u>1.2</u>
III	6	4.3	80.1	2.3
IV	6	4.3	84.7	2.3

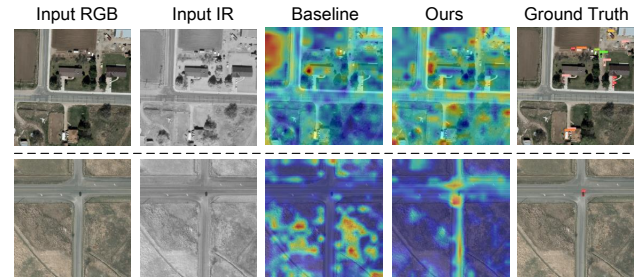


Fig. 7. Comparison of Grad-CAM heatmaps generated from the SS2D layer for the baseline and our method.

This decomposition, however, results in a significant accuracy drop of 6.0% mAP₅₀ compared to the baseline (Row No. I). This indicates that low-rank decomposition alone cannot preserve high-fidelity feature representations. Upon integrating structure-aware distillation (Row No. III and No. IV), we observe substantial performance gains. Notably, the distilled student model not only achieves a significant speedup in inference. It increases from 0.4 FPS to 2.3 FPS on Raspberry Pi 5. When combined with fine-tuning, this model also surpasses the baseline accuracy by 3.2% mAP₅₀ (Row No. IV vs. Row No. I). This suggests that the distillation process effectively transfers the complex spatial-spectral correlations from the original SS2D layers into the compact low-rank counterparts.

Compared with the original baseline, the model optimized with our structure-aware distillation exhibits more concentrated, semantically consistent activation patterns. This indicates that our method enables the low-rank model to better focus on discriminative object features, explaining the observed quantitative improvements in detection accuracy. As shown in Fig. 7.

VI. CONCLUSION AND FUTURE WORK

In this paper, we present an efficient multispectral object detection framework based on 2D Selective Structured State Space (SS2D) models, specifically optimized for edge deployment. First, we propose the Low-Rank SS2D backbone, which reconstructs the vanilla full-rank SS2D via matrix factorization. This design achieves significant model compression while preserving linear complexity and global receptive fields. Second, to alleviate the representation degradation incurred by low-rank approximation, we introduce a Structure-Aware Distillation strategy. By aligning the singular components and

hidden-state dynamics between the full-rank teacher and the low-rank student, our method recovers critical fine-grained structural information for detection. Extensive experiments across five benchmarks and diverse hardware platforms, ranging from high-end GPUs to resource-constrained edge devices, demonstrate that our approach achieves competitive accuracy with significantly enhanced inference efficiency. Future work will explore adaptive low-rank configurations to further push the Pareto frontier of efficiency and precision on the edge.

REFERENCES

- [1] M. Chen, J. Sun, K. Aida, and A. Takefusa, "Weather-aware object detection method for maritime surveillance systems," *Future Generation Computer Systems*, vol. 151, pp. 111–123, 2024.
- [2] L. Wen, Y. Cheng, Y. Fang, and X. Li, "A comprehensive survey of oriented object detection in remote sensing images," *Expert Systems with Applications*, vol. 224, p. 119960, 2023.
- [3] L. Izquierdo-Horna, J. Zevallos, and M. Angulo, "Strategic monitoring of improperly disposed urban waste using uav imagery and object detection," *Resources, Conservation & Recycling Advances*, p. 200306, 2026.
- [4] J. Zhang, J. Lei, W. Xie, Z. Fang, Y. Li, and Q. Du, "Superyolo: Super resolution assisted object detection in multimodal remote sensing imagery," *IEEE Transactions on Geoscience and Remote Sensing*, vol. 61, pp. 1–15, 2023.
- [5] L. Zhang, Z. Liu, S. Zhang, X. Yang, H. Qiao, K. Huang, and A. Husain, "Cross-modality interactive attention network for multispectral pedestrian detection," *Information Fusion*, vol. 50, pp. 20–29, 2019.
- [6] H. Zhang, E. Fromont, S. Lefèvre, and B. Avignon, "Guided attentive feature fusion for multispectral pedestrian detection," in *Proceedings of the IEEE/CVF winter conference on applications of computer vision*, 2021, pp. 72–80.
- [7] Y. Zeng, T. Liang, Y. Jin, and Y. Li, "Mmi-det: Exploring multi-modal integration for visible and infrared object detection," *IEEE Transactions on Circuits and Systems for Video Technology*, vol. 34, no. 11, pp. 11 198–11 213, 2024.
- [8] Z. Wu, Y. Zhang, T. Lu, K. Zhao, and J. Wang, "Contour-texture preservation transformer for face super-resolution," *Neurocomputing*, vol. 626, p. 129549, 2025.
- [9] A. Gu and T. Dao, "Mamba: Linear-time sequence modeling with selective state spaces," *arXiv preprint arXiv:2312.00752*, 2023.
- [10] Y. Liu, Y. Tian, Y. Zhao, H. Yu, L. Xie, Y. Wang, Q. Ye, J. Jiao, and Y. Liu, "VMamba: Visual state space model," in *The Thirty-eighth Annual Conference on Neural Information Processing Systems*, 2024. [Online]. Available: <https://openreview.net/forum?id=ZgtLQQR1K7>
- [11] W. Hua and Q. Chen, "A survey of small object detection based on deep learning in aerial images," *Artificial Intelligence Review*, vol. 58, no. 6, p. 162, 2025.
- [12] Y. Huang, R. Qin, G. Zhao, H. Ji, X. Zheng, and Y. Zhong, "Reconstruct multiscale features for lightweight small object detection in remote sensing images," *IEEE Transactions on Geoscience and Remote Sensing*, vol. 63, pp. 1–15, 2025.
- [13] Y. Zhang, W. Wang, M. Ye, J. Yan, and R. Yang, "Lga-yolo for vehicle detection in remote sensing images," *IEEE Journal of Selected Topics in Applied Earth Observations and Remote Sensing*, 2025.
- [14] L. Wang, J. Li, J. Zhang, L. Zhuo, and Q. Tian, "Position guided dynamic receptive field network: A small object detection friendly to optical and sar images," *IEEE Transactions on Circuits and Systems for Video Technology*, 2025.
- [15] C. Hao, Z. Li, Y. Zhang, W. Chen, and Y. Zou, "Infrared small target detection based on adaptive size estimation by multidirectional gradient filter," *IEEE Transactions on Geoscience and Remote Sensing*, vol. 62, pp. 1–15, 2024.
- [16] L. Tang, H. Zhang, H. Xu, and J. Ma, "Rethinking the necessity of image fusion in high-level vision tasks: A practical infrared and visible image fusion network based on progressive semantic injection and scene fidelity," *Information Fusion*, vol. 99, p. 101870, 2023.
- [17] J. Shen, Y. Chen, Y. Liu, X. Zuo, H. Fan, and W. Yang, "Icafusion: Iterative cross-attention guided feature fusion for multispectral object detection," *Pattern Recognition*, vol. 145, p. 109913, 2024.
- [18] M. Yuan and X. Wei, "C²former: Calibrated and complementary transformer for rgb-infrared object detection," *IEEE Transactions on Geoscience and Remote Sensing*, vol. 62, pp. 1–12, 2024.
- [19] K. Hu, Y. He, Y. Li, J. Zhao, S. Chen, and Y. Kang, "Ei 2 det: Edge-guided illumination-aware interactive learning for visible-infrared object detection," *IEEE Transactions on Circuits and Systems for Video Technology*, 2025.
- [20] J. Zhu, H. Zhang, S. Li, S. Wang, and H. Ma, "Cross teaching-enhanced multi-spectral remote sensing object detection with transformer," *IEEE Journal of Selected Topics in Applied Earth Observations and Remote Sensing*, 2024.
- [21] Y. Zhang, J. Chen, J. Wang, D. Shi, S. Han, and L. Deng, "C2dff-net for object detection in multimodal remote sensing images," *IEEE Transactions on Geoscience and Remote Sensing*, vol. 63, pp. 1–16, 2025.
- [22] H. Li, L. Xiao, L. Cao, D. Wu, Y. Liu, Y. Li, Y. Zhang, and H. Bao, "Crossmodalnet: A dual-modal object detection network based on cross-modal fusion and channel interaction," *Expert Systems with Applications*, p. 129677, 2025.
- [23] T. Qi, J. Tian, Z. Liu, and H. Chen, "Small target detection in remote sensing images based on multi-scale self-attention aggregation and coordinate attention enhancement," *Array*, p. 100724, 2026.
- [24] C. Yue, Y. Zhang, J. Yan, Z. Luo, Y. Liu, and P. Guo, "Diffusion mechanism and knowledge distillation object detection in multimodal remote sensing imagery," *IEEE Transactions on Geoscience and Remote Sensing*, 2025.
- [25] A. Gu, K. Goel, and C. Re, "Efficiently modeling long sequences with structured state spaces," in *International Conference on Learning Representations*, 2022. [Online]. Available: <https://openreview.net/forum?id=uYLFozIvIAC>
- [26] L. Zhu, B. Liao, Q. Zhang, X. Wang, W. Liu, and X. Wang, "Vision mamba: Efficient visual representation learning with bidirectional state space model," *arXiv preprint arXiv:2401.09417*, 2024.
- [27] J. Li, C. Sui, S. Jia, and C. Guo, "Multispectral object detection via cross-modality gated interaction mamba," in *2025 6th International Conference on Internet of Things, Artificial Intelligence and Mechanical Automation (IoTAIMA)*. IEEE, 2025, pp. 155–158.
- [28] M. Zhou, T. Li, C. Qiao, D. Xie, G. Wang, N. Ruan, L. Mei, Y. Yang, and H. T. Shen, "Dmm: Disparity-guided multispectral mamba for oriented object detection in remote sensing," *IEEE Transactions on Geoscience and Remote Sensing*, 2025.
- [29] Y. Feng, S. Jing, Y. Zhao, H. Lv, Y. Zhang, and M. Sun, "Mvmamba: A multiscale vision mamba based on state-space duality for remote sensing object detection," *IEEE Geoscience and Remote Sensing Letters*, vol. 23, pp. 1–5, 2025.
- [30] M. Huh, H. Mobahi, R. Zhang, B. Cheung, P. Agrawal, and P. Isola, "The low-rank simplicity bias in deep networks," *URL http://arxiv.org/abs/2103.10427*, 2023.
- [31] S. M. Kwon, Z. Zhang, D. Song, L. Balzano, and Q. Qu, "Efficient low-dimensional compression of overparameterized models," *arXiv preprint arXiv:2311.05061*, 2024.
- [32] Y. Li, Y. Yu, Q. Zhang, C. Liang, P. He, W. Chen, and T. Zhao, "Losparse: Structured compression of large language models based on low-rank and sparse approximation," in *International Conference on Machine Learning*. PMLR, 2023, pp. 20 336–20 350.
- [33] Y.-C. Hsu, T. Hua, S. Chang, Q. Lou, Y. Shen, and H. Jin, "Language model compression with weighted low-rank factorization," in *International Conference on Learning Representations*, 2022. [Online]. Available: <https://openreview.net/forum?id=uPv9Y3gmA15>
- [34] R. Feng, K. Zheng, Y. Huang, D. Zhao, M. Jordan, and Z.-J. Zha, "Rank diminishing in deep neural networks," *Advances in Neural Information Processing Systems*, vol. 35, pp. 33 054–33 065, 2022.
- [35] G. Hinton, O. Vinyals, and J. Dean, "Distilling the knowledge in a neural network," *arXiv preprint arXiv:1503.02531*, 2015.
- [36] A. Moslemi, A. Briskina, Z. Dang, and J. Li, "A survey on knowledge distillation: Recent advancements," *Machine Learning with Applications*, vol. 18, p. 100605, 2024.
- [37] N. Zeng, X. Li, P. Wu, H. Li, and X. Luo, "A novel tensor decomposition-based efficient detector for low-altitude aerial objects with knowledge distillation scheme," *IEEE/CAA Journal of Automatica Sinica*, vol. 11, no. 2, pp. 487–501, 2024.
- [38] J. Xue, J. Li, Y. Han, Z. Wang, C. Deng, and T. Xu, "Feature-based knowledge distillation for infrared small target detection," *IEEE Geoscience and Remote Sensing Letters*, vol. 21, pp. 1–5, 2024.
- [39] G. Huang, A. Shen, Y. Hu, J. Du, J. Hu, and Y. Liang, "Optimizing yolov5s object detection through knowledge distillation algorithm," in *2024 5th International Conference on Big Data, Artificial Intelligence and Internet of Things Engineering (ICBAIE)*. IEEE, 2024, pp. 80–84.
- [40] L. Zhang, X. Zhang, and Y. Gu, "Knowledge distillation based lightweight satellite video motion target detection algorithm," in *IGARSS*

2025-2025 *IEEE International Geoscience and Remote Sensing Symposium*. IEEE, 2025, pp. 6592–6595.

- [41] G. Jocher, A. Chaurasia, and J. Qiu, “Ultralytics yolov8,” 2023. [Online]. Available: <https://github.com/ultralytics/ultralytics>
- [42] Q. Zhang, W. Wang, Y. Liu, L. Zhou, H. Zhao, J. An, and Z. Wang, “Selective structured state space for multispectral-fused small target detection,” *arXiv preprint arXiv:2505.14043*, 2025.
- [43] S. Razakarivony and F. Jurie, “Vehicle detection in aerial imagery: A small target detection benchmark,” *Journal of Visual Communication and Image Representation*, vol. 34, pp. 187–203, 2016.
- [44] H. Zhang, E. Fromont, S. Lefevre, and B. Avignon, “Multispectral fusion for object detection with cyclic fuse-and-refine blocks,” in *2020 IEEE International conference on image processing (ICIP)*. IEEE, 2020, pp. 276–280.
- [45] X. Jia, C. Zhu, M. Li, W. Tang, and W. Zhou, “Lvip: A visible-infrared paired dataset for low-light vision,” in *Proceedings of the IEEE/CVF international conference on computer vision*, 2021, pp. 3496–3504.
- [46] J. Liu, X. Fan, Z. Huang, G. Wu, R. Liu, W. Zhong, and Z. Luo, “Target-aware dual adversarial learning and a multi-scenario multi-modality benchmark to fuse infrared and visible for object detection,” in *Proceedings of the IEEE/CVF conference on computer vision and pattern recognition*, 2022, pp. 5802–5811.
- [47] Y. Sun, B. Cao, P. Zhu, and Q. Hu, “Drone-based rgb-infrared cross-modality vehicle detection via uncertainty-aware learning,” *IEEE Transactions on Circuits and Systems for Video Technology*, vol. 32, no. 10, pp. 6700–6713, 2022.
- [48] I. Sutskever, J. Martens, G. Dahl, and G. Hinton, “On the importance of initialization and momentum in deep learning,” in *International conference on machine learning*. PMLR, 2013, pp. 1139–1147.
- [49] X. Wu, L. Wang, J. Guan, H. Ji, L. Xu, Y. Hou, and A. Fei, “Dhanet: Dual-stream hierarchical interaction networks for multimodal drone object detection,” *IEEE Transactions on Geoscience and Remote Sensing*, 2025.
- [50] H. Fu, H. Liu, J. Yuan, X. He, J. Lin, and Z. Li, “Yolo-adaptor: A fast adaptive one-stage detector for non-aligned visible-infrared object detection,” *IEEE Transactions on Intelligent Vehicles*, 2024.
- [51] Z. Zhao, H. Bai, J. Zhang, Y. Zhang, S. Xu, Z. Lin, R. Timofte, and L. Van Gool, “Cddfuse: Correlation-driven dual-branch feature decomposition for multi-modality image fusion,” in *Proceedings of the IEEE/CVF conference on computer vision and pattern recognition*, 2023, pp. 5906–5916.
- [52] L. Tang, J. Yuan, H. Zhang, X. Jiang, and J. Ma, “Piafusion: A progressive infrared and visible image fusion network based on illumination aware,” *Information Fusion*, vol. 83, pp. 79–92, 2022.
- [53] W. Tang, F. He, Y. Liu, Y. Duan, and T. Si, “Datfuse: Infrared and visible image fusion via dual attention transformer,” *IEEE Transactions on Circuits and Systems for Video Technology*, vol. 33, no. 7, pp. 3159–3172, 2023.
- [54] Y. Zhang, Y. Liu, P. Sun, H. Yan, X. Zhao, and L. Zhang, “Ifcnn: A general image fusion framework based on convolutional neural network,” *Information Fusion*, vol. 54, pp. 99–118, 2020.
- [55] F. Qingyun and W. Zhaokui, “Cross-modality attentive feature fusion for object detection in multispectral remote sensing imagery,” *Pattern Recognition*, vol. 130, p. 108786, 2022.
- [56] B. Cao, Y. Sun, P. Zhu, and Q. Hu, “Multi-modal gated mixture of local-to-global experts for dynamic image fusion,” in *Proceedings of the IEEE/CVF international conference on computer vision*, 2023, pp. 23 555–23 564.
- [57] L. Tang, X. Xiang, H. Zhang, M. Gong, and J. Ma, “Divfusion: Darkness-free infrared and visible image fusion,” *Information Fusion*, vol. 91, pp. 477–493, 2023.
- [58] G. Xu, C. He, H. Wang, H. Zhu, and W. Ding, “Dm-fusion: Deep model-driven network for heterogeneous image fusion,” *IEEE transactions on neural networks and learning systems*, vol. 35, no. 7, pp. 10071–10085, 2023.
- [59] L. Zhang, Z. Liu, X. Zhu, Z. Song, X. Yang, Z. Lei, and H. Qiao, “Weakly aligned feature fusion for multimodal object detection,” *IEEE Transactions on Neural Networks and Learning Systems*, 2021.
- [60] M. Yuan, Y. Wang, and X. Wei, “Translation, scale and rotation: cross-modal alignment meets rgb-infrared vehicle detection,” in *European Conference on Computer Vision*. Springer, 2022, pp. 509–525.
- [61] J. Han, J. Ding, J. Li, and G.-S. Xia, “Align deep features for oriented object detection,” *IEEE transactions on geoscience and remote sensing*, vol. 60, pp. 1–11, 2021.
- [62] K. Zhou, L. Chen, and X. Cao, “Improving multispectral pedestrian detection by addressing modality imbalance problems,” in *European conference on computer vision*. Springer, 2020, pp. 787–803.



Qianqian Zhang is currently a Ph.D. candidate specializing in Computer Application Technology at the University of Chinese Academy of Sciences (UCAS), Beijing, China. Supported by the China Scholarship Council, she is also conducting joint training and collaboration with Queen Mary University of London, London, United Kingdom.

Her research interests focus on large visual models, multimodal fusion, object detection, model lightweighting, efficient deployment, and video compression.



Leon Tabaro is currently a Ph.D. candidate at the School of Electronic Engineering and Computer Science, Queen Mary University of London, London, UK. His research interests lie at the intersection of geometric deep learning, machine learning systems and optimization, with a focus on general purpose deep sequence models with long-range memory, efficient training and inference, and structured sparsity for compact deep learning models.



Ahmed M. Abdelmoniem (Senior Member, IEEE) is an Associate Professor at the School of Electronic Engineering and Computer Science, Queen Mary University of London, UK, and leads SAYED Systems Group. He held the positions of Research Scientist at KAUST, Saudi Arabia, and Senior Researcher at Huawei’s Future Networks Lab (FNTL), Hong Kong. He is the principal investigator and co-investigator on several national and international research projects, funded mainly by grants totaling over USD\$1.8 million. He received his PhD in

Computer Science and Engineering from the Hong Kong University of Science and Technology, Hong Kong, in 2017. He was awarded the prestigious Hong Kong PhD Fellowship from the RGC of Hong Kong in 2013 to pursue his PhD at HKUST, HK. He has published numerous (more than 135) papers in top venues and journals in distributed systems, computer networking, and machine learning. His current research interests are optimizing systems supporting distributed machine learning, federated learning, and cloud/data-center networking, emphasizing performance, practicality, and scalability.



Junshe An received the Bachelor of Science degree from Beihang University, Beijing, China, in 1992, the Master of Science degree from the University of Science and Technology Beijing, Beijing, China, in 1995, and the Doctor of Philosophy degree from Northwestern Polytechnical University, Xi’an, China, in 2004. He is currently a Researcher with the National Space Science Center, Chinese Academy of Sciences, Beijing, China.

His research interests focus on space-integrated electronic technologies, including aerospace computer hardware and software, system architecture, and intelligent information processing.